Systematics of $K\alpha$ x-ray satellite structure

V. Horvat,* R. L. Watson, and Yong Peng
Cyclotron Institute and Department of Chemistry, Texas A&M University, College Station, Texas 77843-3366, USA
(Received 11 June 2006; published 17 August 2006)

Spectra of K x rays emitted from a variety of solid targets (atomic number $Z_2=17-32$) under bombardment by fast heavy ions (atomic number $Z_1=6-83$) at 2.5–25 MeV/amu were measured in high resolution using a curved crystal spectrometer. The spectra were analyzed in order to examine the dependence of $K\alpha$ x-ray satellite structure on the Geometrical Model's universal variable X_n. Scaling rules were established for the apparent average L-shell spectator vacancy fraction at the time of $K\alpha$ x-ray emission, the satellite peak centroids, and the satellite peak widths.

DOI: 10.1103/PhysRevA.74.022718 PACS number(s): 34.50.Fa, 32.30.Rj

I. INTRODUCTION

K-shell ionization of a target atom by a fast heavy ion is likely to be accompanied by multiple L-shell and outer-shell (M, N,…) ionization and excitation. The decay of such a state typically results in a series of radiative (x ray) and nonradiative (Auger and Coster-Kronig) transitions. The energy of an x ray photon emitted in a radiative transition depends primarily on the initial and final quantum numbers of the active electron, but it also depends on the number of spectator vacancies and their configuration, as well as on the coupling of electronic angular momenta in the initial and final states. Compared to the corresponding diagram K x rays (emitted by single-vacancy atoms), the energies of K x-ray photons emitted by multiply ionized atoms generally increase as the number of spectator vacancies increases. K x-ray energy shifts due to the presence of a spectator L vacancy are much larger than those due to the presence of an outer-shell spectator vacancy, so that the spectrum of K x rays measured using a high-resolution spectrometer often displays a structure in which individual peaks (known as the K x-ray satellites) correspond to a specific number (i) of spectator L vacancies involved in the underlying transitions. These peaks can be labeled as $K\xi L^i$, where ξ denotes the transition type (i.e., $\xi=\alpha$ or β). $K\alpha$ x rays are those emitted in $2p\rightarrow 1s$ transitions of the active electron, while $K\beta$ x rays correspond to transitions into the K shell from outer shells. Variations in the number and configuration of outer-shell vacancies as well as variations in the coupling of electron angular momenta result in broadening of the $K\xi L^i$ peaks and determine how well they can be resolved.

Due to the spin-orbit coupling of electron angular momenta in the initial state, the $K\alpha$ transitions in single-vacancy atoms give rise to two peaks, commonly labeled as $K\alpha_1$ and $K\alpha_2$, corresponding to $2p_{3/2}\rightarrow 1s$ and $2p_{1/2}\rightarrow 1s$ transitions, respectively. Their intensity ratio is very close to 2:1, as expected statistically based on the number of available $2p$ electrons in the initial states. The two peaks may or may not be resolved, depending on how their separation compares to their natural line width and the resolution of the spectrometer. Similar splitting is expected to determine the structure of the $K\alpha$ x-ray satellite peaks, although the two components are seldom resolved [1,2].

In the past, the distribution of intensities I_i of the $K\alpha L^i$ peaks as a function of i has been successfully described using a binomial distribution

$$I_i = I_{tot}\binom{8}{i}(p_L^x)^i(1-p_L^x)^{8-i}, \tag{1}$$

where

$$I_{tot} = \sum_{i=0}^{8} I_i. \tag{2}$$

The parameter of this distribution (p_L^x) can be interpreted as the apparent average L-shell spectator vacancy fraction at the time of $K\alpha$ x-ray emission and expressed by

$$p_L^x = \frac{1}{8}\sum_{i=1}^{8}(iI_i)/I_{tot}. \tag{3}$$

In this work, Eq. (3) is used as a model-independent *definition* of p_L^x, because neither its value nor its interpretation depend on the actual distribution of I_i. The true average L-shell spectator vacancy fraction at the time of x-ray emission can be determined using the same expression after correcting the measured satellite peak intensities for the i dependence of fluorescence yield. When the measured satellite peak intensities are also corrected for target vacancy rearrangement between the time of collision and the time of x-ray emission, the right-hand side of Eq. (3) yields the average L-shell spectator vacancy fraction at the time of collision (p_L).

The dependence of p_L (or p_L^x) on the collision parameters (i.e., atomic number Z_1, speed v_1 and charge q_1 of the projectile and average speed v_2 of the target electron) has been studied since the 1970's. Schmiedekamp *et al.* [3] measured the dependence on Z_1 and v_1 of p_L for Ar gas target atoms bombarded by 1–5 MeV/amu projectiles with atomic numbers 1–17. They proposed a semiempirical scaling rule that takes into account the increased binding of the target electron due to the presence of the projectile. Another scaling rule, proposed by Watson *et al.* [4], was based on the measurements involving solid and gas targets and also included the dependence on v_2. Beyer *et al.* [5] have found that for fully

*Electronic address: V-Horvat@tamu.edu

stripped light projectiles and for highly stripped heavy ions, p_L for a gas target is a linear function of v_1/q_1.

The practical usefulness of the proposed semiempirical scaling rules [3–5] for predicting the value of p_L for an arbitrary collision system is limited, mainly for the following two reasons: (a) the parameters in the proposed semiempirical formulas were derived from a scarce amount of experimental data, and in some cases from one set of measurements, (b) the experimental values of p_L were determined from the spectra of x rays by different authors using different methods of peak fitting and applying different approaches to corrections for the i dependence of fluorescence yield and for target vacancy rearrangement between the time of collision and the time of x-ray emission.

A comprehensive theoretical approach to the systematics of p_L, known as the Geometrical Model (GM), was developed by Sulik [6]. This model involves a free target atom (which implies that the results apply to gas targets better than to solid targets), and it includes only direct ionization as a mechanism for target vacancy production. The model predicts that in the target atom shell having principal quantum number n $(n=1,2,3..)$, the corresponding spectator vacancy fraction $(p_n, n=1(K),2(L),3(M),\ldots)$, produced at the time of collision is a function of a universal variable X_n, given by

$$X_n = 4V[G(V)]^{1/2}Z_1/(nv_1), \tag{4}$$

where $V=v_1/v_2$ is the scaled projectile speed and $G(V)$ is the binary encounter approximation (BEA) function [7] originally formulated to describe the universal scaling of cross sections for inner-shell ionization. The values of p_n predicted by the GM depend on which one of the several proposed forms of $G(V)$ is used and whether Z_1 is interpreted as the projectile atomic number or as an effective screened projectile charge. In the latter case, the results also depend on how the projectile charge is calculated.

In the work presented here, spectra of K x rays emitted from a variety of solid targets $(Z_2=17-32)$ under bombardment by fast heavy ions $(Z_1=6-83)$ at 2.5–25 MeV/amu were measured using a curved crystal spectrometer. Based on a large number of x-ray spectra that were measured and analyzed in a consistent way, the dependence of p_L^x on the universal variable X_n [6] was established. The results are compared with the predictions of the Geometrical Model.

The systematics of p_L^x rather than that of p_L were studied because p_L^x can be determined directly from the measured spectra in a straight-forward way and with greater accuracy [based on Eq. (3)]. On the other hand, corrections due to the i dependence of fluorescence yield and target vacancy rearrangement between the time of collision and the time of x-ray emission can be substantial, while their accuracy is limited because the calculations involved are complex and model dependent. Since different approximations are applied by different authors, choosing one method over another would decrease the practical value of the results and potentially increase the systematic error.

Also studied were the systematics of the $K\alpha$ satellite peak centroids and widths, as obtained in the analysis of the measured x-ray spectra. The aim was to complete the set of semiempirical scaling laws that can be used to predict the structure of $K\alpha$ x-ray spectra for solid targets bombarded by heavy ions. The formulas that were derived should facilitate the analysis of x-ray spectra in which the satellite peaks are not resolved.

II. EXPERIMENT

Beams of heavy ions $(Z_1=6-83)$ at 2.5–25 MeV/amu were extracted from the Texas A&M K-500 superconducting cyclotron, charge analyzed, collimated, and focused to a ~3 mm diam spot onto the target oriented at 45° with respect to the beam direction. The focusing was accomplished with the aid of a zinc/cadmium sulfide phosphor and a closed circuit television system. During the data acquisition, the beam intensity was monitored by measuring the current from the target or from a Faraday cup placed directly behind the target.

The targets included pellets of KCl and a mixture of Ge and graphite, as well as metallic foils of Ti, V, Fe, Co, Ni, and Cu. A few of the targets were thick enough to stop the beam. However, because of K x-ray absorption and the projectile energy dependence of K x-ray production, the estimated effective mean target depth for target K x-ray detection in these cases was on the order of several mg/cm^2. Typically, the effective mean projectile energy was estimated to be about 10% below the incident value. The effects of projectile energy loss on the spectral features of interest were studied by performing additional measurements using a range of target thicknesses and were found to be small and predictable.

A 12.7 cm Johansson-type curved crystal spectrometer with its focal circle oriented perpendicular to the beam axis was used to measure the x-ray spectra. X rays emitted from the target were diffracted from the crystal in first order (for $Z_2=17-26$) or in the second order (for $Z_2=27-32$) and counted by a flow proportional counter operating with P-10 gas [argon (90%) and methane (10%)] at 1 atm. A NaCl crystal was used in the measurements of Cl K x rays, while a LiF(200) crystal was used for all other measurements. Control of the spectrometer stepping motor was accomplished by means of a custom-designed electronic module and a personal computer equipped with a dedicated multiscaler expansion card and the accompanying software. Before each run series, the crystal angle and focal circle were manually adjusted to maximize the intensity of the measured K x rays.

The energy scale was initially determined for each measured spectrum using the recommended transition energies of Deslattes *et al.* [8] and the *estimated* centroids of the peaks due to $K\alpha_1$ and $K\beta_1$ diagram x rays (emitted from target atoms with a single vacancy). This energy scale was refined in the final analysis of the spectrum, in which a more elaborate procedure was used to determine the peak centroids. Diagram x rays are quite prominent when a target is bombarded by heavy ions [9,10]. Single-vacancy configurations are produced primarily by high-energy electrons ejected in the primary collisions or by high-energy photons subsequently emitted from the projectile or the target.

The energy resolution of the spectrometer varied somewhat, depending on the quality of the beam focus and the

crystal and focal circle alignment. Its average value, expressed in terms of the full width at half maximum (FWHM), was determined from the Gaussian component widths of the Voigt functions that were used to fit the $K\alpha_1$ peaks. The average energy resolution was found to be 8.3 eV for Cl, 6.6 eV for K, 11.5 eV for Ti, 14.6 eV for V, 6.5 eV for Co (second order), 8.5 eV for Ni (second order), and 10.3 eV for Cu (second order).

III. INTERPRETATION OF THE SPECTRA

The gross features of the $K\alpha$ region of the x-ray spectrum are shown in Fig. 1 for a Co target. The $K\alpha_1$ and $K\alpha_2$ diagram x-ray energies [8] are marked by the vertical dashed lines. Within ±1 eV or less, they were found to agree with the estimated centroids of the corresponding peaks, determined in the preliminary energy calibration (explained in Sec. II). The shape of the diagram peaks was found to be accurately represented by a Voigt function, while the Lorentzian component widths agreed well with the natural line widths derived from the recommended level widths of Campbell and Papp [11]. Consequently, the latter values were used as fixed parameters in the peak-fitting analysis of the spectra. The relative intensities of the diagram peaks were treated likewise, since they agreed well with the relative transition rates recommended by Salem, Panossian, and Krause [12]. The spectra of x rays emitted from the other targets were found to have the same qualities and were analyzed in the same way.

Target atom K-shell ionization by heavy ions is most commonly accompanied by the removal of electrons from outer shells. Consequently, K x rays emitted from multiply ionized target atoms (K x-ray satellites) give rise to peaks that are broadened and shifted relative to those corresponding to transitions in single-vacancy atoms. Furthermore, the satellite peak shapes can be very complex due to variations in the initial state vacancy configuration at the time of x-ray emission and the complicated multiplet structure that arises from the coupling of initial and final state angular momenta. In Co, according to calculations performed using the multiconfigurational Dirac-Fock (MCDF) code of Desclaux [13], the $K\alpha$ satellite transition energies are shifted (on the average) by only a few eV per outer-shell vacancy (2.1 to 2.7 eV for a single spectator M vacancy), which is comparable to the natural width of the transitions involved (2.4 eV for $K\alpha_1$). Consequently, peaks due to K x-ray transitions from initial states involving a single K vacancy, plus multiple outer shell vacancies (but no L vacancies), cannot be resolved from each other or from the corresponding diagram peaks. Therefore, the structure observed in the vicinity of the diagram transition energy includes contributions both from diagram transitions in atoms ionized by secondary radiation and from satellite transitions in atoms that acquire a single K-shell and multiple outer-shell vacancies in collisions with heavy ions. Apparently, the $K\alpha$ x rays that predominantly contribute to the $K\alpha L^0$ peaks of the spectra shown in Fig. 1 are emitted in the presence of a small number of outer-shell vacancies. This is evidenced by relatively small energy shifts of the $K\alpha L^0$ satellites from the corresponding diagram transition energies and a negligible increase in their widths compared to the corresponding diagram peaks.

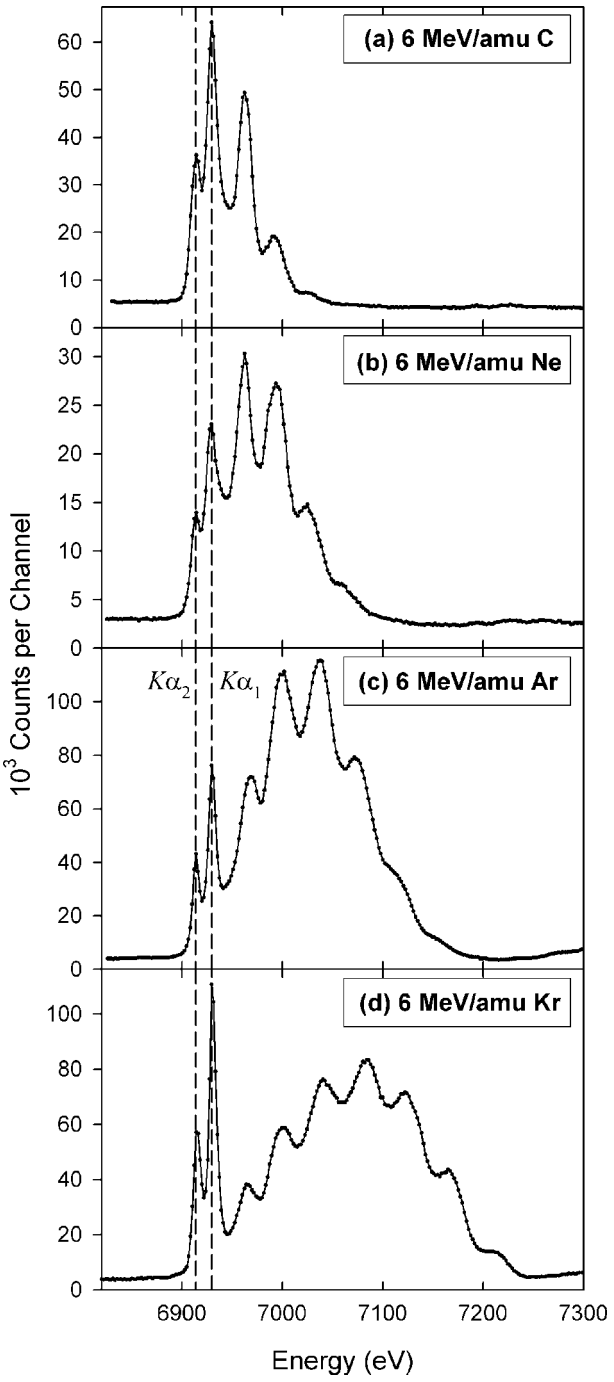

FIG. 1. Spectra of K x rays emitted from a thick metallic Co target under bombardment by 6 MeV/amu beams of (a) C, (b) Ne, (c) Ar, and (d) Kr. The vertical dashed lines indicate the energy positions of the $K\alpha_1$ and $K\alpha_2$ diagram lines.

If, on the other hand, K-shell ionization induced by heavy ions is also accompanied by single or multiple L-shell ionization, the resulting satellite peaks are additionally shifted up in energy. In Co, this additional shift per L vacancy for $K\alpha$ transitions amounts to 28 eV or more. The satellite peaks may or may not be resolved, depending on how their shifts compare with their widths. For a given number of spectator L

vacancies, the corresponding satellite peak width depends, for the most part, on the average number of outer-shell vacancies and the extent of multiplet splitting.

$K\alpha$ x-ray satellite peaks are the dominant feature appearing in the spectra obtained with Ne, Ar, and Kr ions [shown in Figs. 1(b)–1(d), respectively]. The same is true for spectra obtained with heavier ions (not shown). As expected, the degree of multiple ionization in the L shell of the target atom increases rapidly with the projectile atomic number. Consequently, the centroids of the satellite peak distributions (including all satellites, regardless of the corresponding number of spectator L vacancies) are shifted higher in energy and the widths of the satellite peak distributions increase. In addition, due to the increased degree of outer-shell ionization and the increasingly complex multiplet structure, satellite peaks corresponding to a given number of spectator L vacancies become broader and are therefore less resolved. Also, the increase in the energy shift of the satellite distribution is larger than the corresponding increase in the distribution width, so that the satellite distribution contributes less in the vicinity of the corresponding diagram transition energies. On the other hand, the contributions from secondary ionization are substantial, and so the peaks due to diagram transitions become more prominent.

The degree of multiple L-shell ionization in the target atom decreases when the projectile energy increases, as demonstrated in Fig. 2 for the case of Ar projectiles and a Ti target. This behavior may be expected because in the present collision regime the speed of the projectiles is much larger than the average speed of target L-shell electrons. In the spectra shown in Fig. 2, the $K\alpha_{1,2}$ doublet is not resolved and the contribution from secondary ionization is relatively small.

IV. ANALYSIS OF THE SPECTRA

Analysis of the spectra focused on the $K\alpha$ transitions. Peaks due to diagram transitions were represented by Voigt functions and their Lorentzian component widths were fixed at the values of the natural line widths obtained from Ref. [11]. The Gaussian component width of the Voigt functions, representing (for the most part) the resolution of the spectrometer, was assumed to be the same for $K\alpha_1$ and $K\alpha_2$ diagram peaks. Its best-fit value was determined for each measured spectrum individually. The diagram peak centroids (on the energy scale) were allowed to have a small common shift from their expected values [8] in order to correct for inaccuracies in the preliminary energy calibration. This feature was especially important in the analysis of spectra in which the diagram peaks were not resolved from the $K\alpha L^1$ satellites. In those cases, the errors in the estimated centroids of the diagram-line peaks were expected to be substantial.

The $K\alpha_1$ and $K\alpha_2$ satellite peaks were also represented by Voigt functions. It was assumed that the centroid shifts of the satellite peaks relative to their corresponding diagram lines were the same for both transition types for a given number (i) of spectator L vacancies. Likewise, it was assumed that the Gaussian component widths of the satellite peaks corresponding to the two transition types were the same for a given i. Otherwise, the values of the satellite peak centroids and their Gaussian component widths were independently optimized in the least squares fits whenever the peaks were at least partially resolved. The results were then used to estimate the centroids and Gaussian component widths of the unresolved peaks. These estimates were used as fixed param-

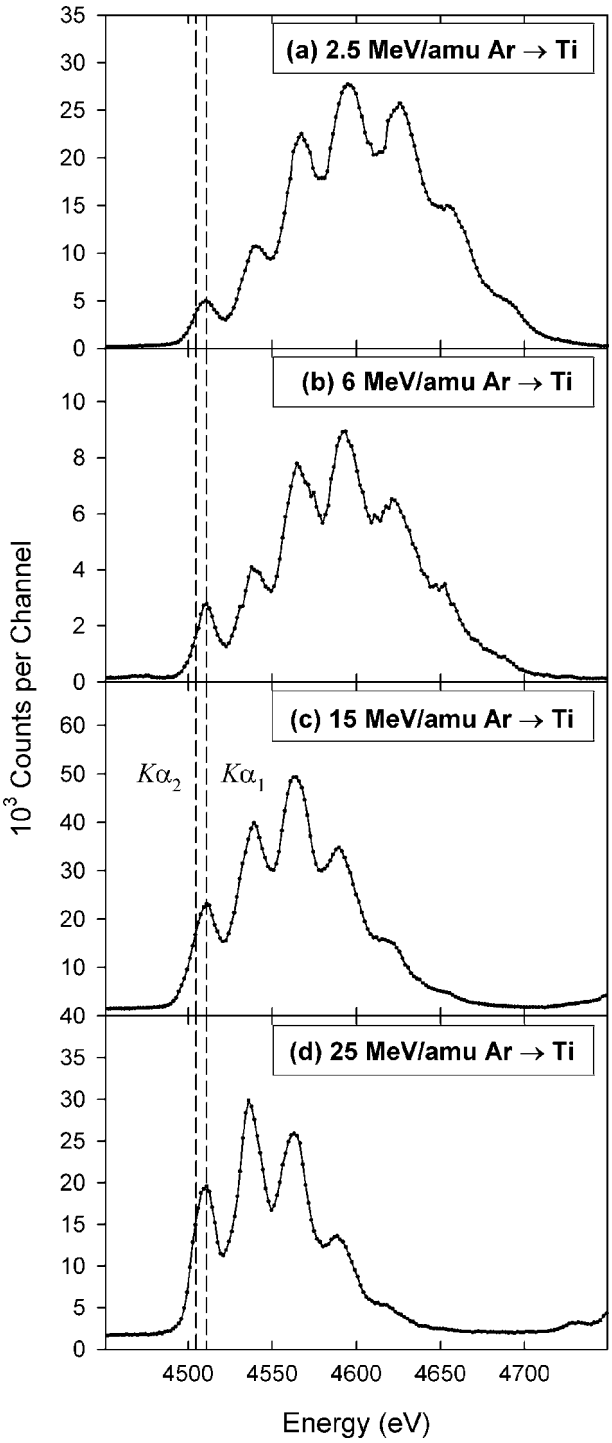

FIG. 2. Spectra of K x rays emitted from a thick metallic Ti target under bombardment by Ar projectiles at (a) 2.5 MeV/amu, (b) 6 MeV/amu, (c) 15 MeV/amu, and (d) 25 MeV/amu. The vertical dashed lines indicate the energy positions of the $K\alpha_1$ and $K\alpha_2$ diagram lines.

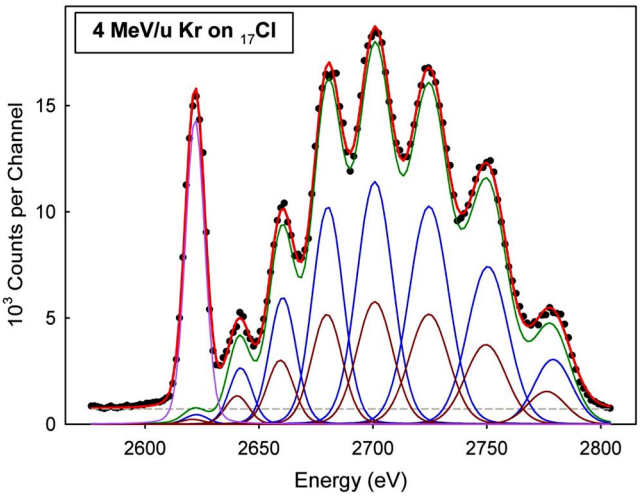

FIG. 3. (Color online) Spectrum of chlorine K x rays emitted from a thick KCl target bombarded by 6 MeV/amu Kr ions. The circles represent the measured data points, while the solid lines represent the overall fit (red), the contributions from $K\alpha_1$ and $K\alpha_2$ satellites (blue and brown, respectively), and the combined contribution from the $K\alpha_1$ and $K\alpha_2$ diagram lines (purple). The dashed line (gray) represents the background.

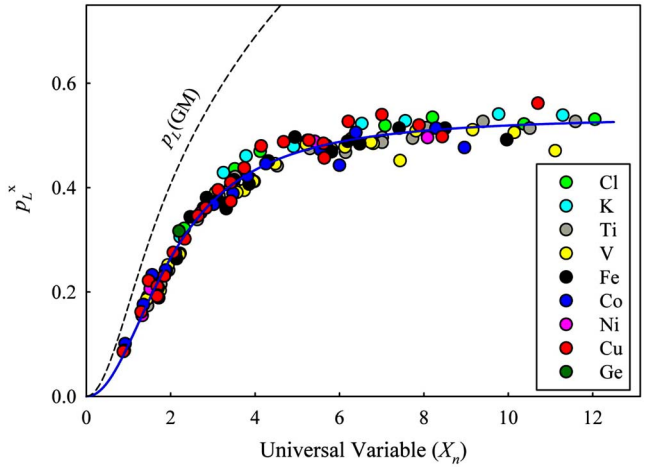

FIG. 4. (Color online) Apparent average L-vacancy fractions at the time of $K\alpha$ x-ray emission (p_L^x), plotted as a function of the universal variable (X_n) determined using Eq. (4) for $n=2$. The data points represent the results of measurements involving a variety of solid targets (atomic number $Z_2=17-32$) under bombardment by fast heavy ions (atomic number $Z_1=6-83$) at 2.5–25 MeV/amu, while the solid line represents the best-fit logistic curve. The dashed curve represents the L-vacancy fractions at the time of collision, predicted by the Geometrical Model [6].

eters in the final analysis. The Lorentzian component widths of the satellite peaks were assumed to be the same as those of the corresponding diagram peaks.

The relative intensities of $K\alpha_1$ and $K\alpha_2$ satellite peaks were assumed to be the same as those for the $K\alpha_1$ and $K\alpha_2$ diagram transitions, respectively (i.e., those from Ref. [12]). This means that the intensities I_i of $K\alpha_1$ and $K\alpha_2$ satellite peaks were assumed to follow the same distribution as a function of i. Whenever possible, the best-fit values of I_i were determined independently from any other parameters of the fit. However, intensities of peaks that were not well-resolved could not be determined in the fitting procedure with sufficient precision. Instead, they were estimated by assuming they followed a binomial distribution that was determined dynamically based on the intensities of two or more well-resolved nearby peaks. This procedure was routinely used to determine the number of counts in the $K\alpha L^0$ satellites, since they overlap with the $K\alpha$ diagram peaks. Finally, the apparent average L-vacancy fraction at the time of $K\alpha$ x-ray emission was calculated using Eq. (3), with $I_8=0$. The background in the spectra shown in Figs. 1(a), 1(b), and 1(d) was parametrized as a linear function of energy although in most cases the slope was fixed at the value of zero. The quality of a typical fit is illustrated in Fig. 3.

In the fitting procedure, the $K\alpha_1 L^0$ and $K\alpha_2 L^0$ satellite peaks were analyzed assuming that their centroids are the same as those of the corresponding diagram peaks. This was done to avoid large statistical errors in the best-fit values of the centroids, Gaussian component widths, and the intensities of these overlapping peaks. Some justification for this assumption comes from the known fact that the $K\alpha L^0$ shift per outer-shell vacancy is small compared to the shift per L vacancy. Additionally, its direction depends on the location of spectator vacancies. For example, a vacancy in a $3d$ orbital causes a negative $K\alpha L^0$ energy shift, while a vacancy in any other outer shell orbital causes a positive energy shift, so that the shifts due to randomly distributed outer-shell vacancies tend to cancel. Also in retrospect, this assumption seems to be justified based on the good quality of a typical fit.

V. RESULTS AND DISCUSSION

A. Apparent average L-shell spectator vacancy fraction at the time of $K\alpha$ x-ray emission

It was found that the measured apparent average L-vacancy fractions (p_L^x) follow a universal curve when plotted as a function of the universal variable X_n defined by Eq. (4) with $n=2$. In the present application, Z_1 was taken to be the projectile nuclear charge, the effective mean value was used for v_1, and v_2 was computed from the neutral atom L_3 binding energy [8]. The form of the function $G(V)$ employed here was one developed by Gryzinski and presented in analytical form in Ref. [14]. The results are shown in Fig. 4 for Z_1 ranging from 6 to 83, v_1 ranging from 9 to 30 a.u., and V ranging from 1.3 to 6.2.

Evidently, the scaling predicted by the Geometrical Model is appropriate, since the measured apparent average vacancy fractions do seem to follow a universal curve as a function of X_n. The solid line in Fig. 4 is a logistic curve that has been fit to 128 data points and represents an empirical universal function for the apparent average spectator L-vacancy fractions. It is given by

$$p_L^x = a/[1 + (b/X_n)^c], \tag{5}$$

where $a=0.537\pm0.006$, $b=2.11\pm0.08$, and $c=2.02\pm0.03$. The values of the parameters of the fit agree well with those obtained previously [15] based on a much smaller sample

that also included the data points for p_M^x and p_{N+}^x. In the present analysis the square of the correlation coefficient (r^2) was 0.973, while the root-mean-square (rms) deviation of the data points from the fitted function was 0.019.

The effective mean value of the projectile speed (v_1) was calculated by taking into account the projectile penetration depth dependence of $K\alpha_1$ x-ray detection on (a) projectile energy, (b) K x-ray production cross section, and (c) x-ray transmission probability. Ziegler's code was used to estimate the projectile energy loss [16], while the x-ray production cross sections were approximated by the combined cross sections for direct ionization and ionization by nonradiative electron capture, calculated according to the perturbed stationary-state theory with corrections for energy loss, Coulomb deflection, and relativistic effects (ECPSSR theory) [17]. The $K\alpha_1$ transition energies were taken from Ref. [8] and the current recommended values [18] were used for the x-ray attenuation coefficients.

If the incident projectile speeds were used in Eq. (4) instead of their effective mean values, the data points shown in Fig. 4 would be shifted to the left by less than 5%. A fit of Eq. (5) to the shifted data points would result in different values of the parameters a, b, and c. However, the differences between the new values and the corresponding old values would be comparable to or less than their errors. The recommended values of p_L^x obtained from Eq. (5) would change by less than 0.00004 (0.05%) on average, with the rms deviation of 0.003 (1%), ranging from −3.4% to 4.1% (−0.005 to 0.010). These deviations are comparable to the typical error of p_L^x.

In the determination of X_n, the average target electron speed prior to ionization (v_2) was calculated from the binding energy of L_3 electrons in neutral atoms [8], since these electrons are the most numerous and have the smallest binding energies of their respective shells. Therefore, at present projectile speeds, they are the most likely to be ionized. If different binding energies were used in Eq. (4), for example, those of L_1 electrons, the values of X_n for the data points shown in Fig. 4 would decrease by 1.8% (for 25 MeV/amu Kr on V) to 7.4% (for 2.5 MeV/amu Xe on Fe), or 3.6% on average.

As pointed out previously [15], the substantial discrepancy at large values of the universal variable between the semiempirical values of p_L^x (shown by the solid line in Fig. 4) and the theoretical values of p_L (shown by the dashed line in Fig. 4) are too large to be accounted for by electronic rearrangement between the time of collision and the time of x-ray emission together with the dependence on i of the fluorescence yield. Possibly, a large fraction of this discrepancy is due to solid state effects (interatomic transitions). To illustrate this point, a spectrum of chlorine $K\alpha$ x rays was measured using Cl_2 gas under bombardment by 6 MeV/u Xe ions. The value obtained for p_L^x was 0.69, which is much larger than the value of 0.52 obtained in the measurement with a KCl target under the same conditions, but still not as large as the theoretical value of p_L (0.96). The two spectra are shown in Fig. 5.

B. $K\alpha$ x-ray satellite peak centroids

The dependence on the measured apparent average L-vacancy fraction (p_L^x) of the measured energy shifts of copper (Cu) $K\alpha L^i$ satellite peaks ($i=1,2,3,4,5,6,7$) relative to the corresponding $K\alpha L^0$ satellite peaks are shown in Fig. 6. Data points are shown only for peaks analyzed without any constraints. For a given i, the satellite energy shifts appear to be linear functions of p_L^x. Similar results were obtained for other targets.

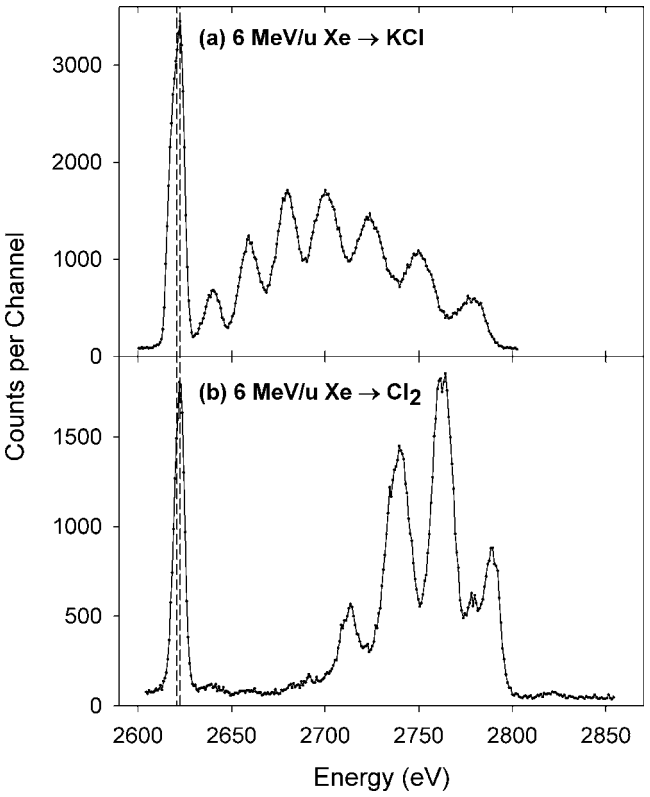

FIG. 5. Spectra of chlorine $K\alpha$ x rays excited by 6 MeV/u Xe ions, measured using (a) a solid KCl target and (b) Cl_2 gas. The latter spectrum shows a significantly higher degree of both L-shell and outer-shell ionization of the target atoms.

It should be noted that the data points in Fig. 6 were determined from spectra taken with a variety of projectiles and collision energies. The fact that the data points deviate from their respective best-fit lines by a relatively small amount indicates that this correlation is independent of projectile atomic number Z_1 and speed v_1. Furthermore, the positive slopes of the best-fit lines in Fig. 6 indicate that the degree of outer-shell ionization increases with the degree of L-shell ionization. This observation is in agreement with the predictions of the Geometrical Model [6].

As p_L^x approaches zero, it seems reasonable to expect that the degree of outer-shell ionization approaches zero as well. The limiting values of the satellite energy shifts (i.e., those in the absence of outer-shell ionization) can be predicted by atomic structure calculations. This was accomplished using the multiconfigurational Dirac-Fock (MCDF) code of Desclaux [13]. The calculated energy shifts were then used to define the ordinate intercepts of the straight lines shown in Fig. 6, while their slopes were determined from the data using linear regression. The slope of each of the seven straight lines in Fig. 6 can be interpreted as the shift due to outer-shell vacancies (ΔE^i) divided by p_L^x, where ΔE^i is the

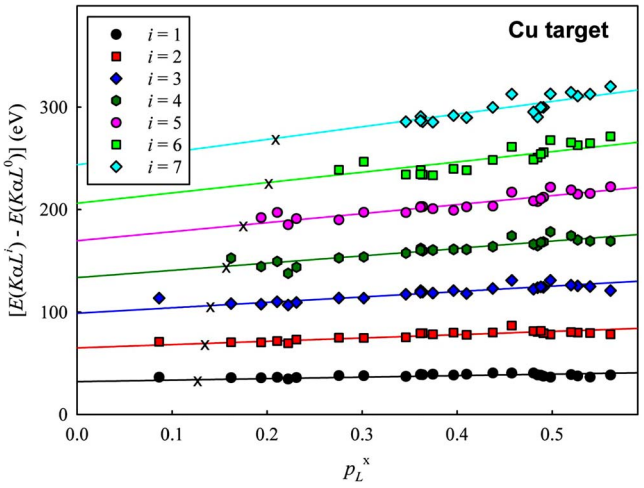

FIG. 6. (Color online) Dependence on the apparent average L-vacancy fraction at the time of $K\alpha$ x-ray emission (p_L^x) of the energy shifts of copper $K\alpha L^i$ satellite peaks ($i=1,2,3,4,5,6,7$) relative to the corresponding $K\alpha L^0$ satellite peaks. Symbols represent the measured data points (weighted averages of $K\alpha_1$ and $K\alpha_2$ shifts), while the solid curves are the corresponding best-fit straight lines intersecting the ordinate at the values predicted by multiconfigurational Dirac-Fock calculations for zero outer-shell vacancies [13]. The crosses represent the predictions of Ref. [19].

difference between the actual energy shift of a $K\alpha$ satellite peak corresponding to i spectator L vacancies and its calculated value in the absence of outer-shell vacancies.

A similar analysis was also applied to the data obtained for six other targets. This resulted in a set of 49 values of $\Delta E^i/p_L^x$. They are plotted in Fig. 7 as a function of i and as a function of the target atomic number (Z_2). Based on the trends observed in the two graphs of Fig. 7, it was found that, with reasonable accuracy, $\Delta E^i/p_L^x$ can be parametrized as

$$\Delta E^i(Z_2)/p_L^x = (i-1)(Z_2 - a') + b', \tag{6}$$

where a', and b' are constants. Their best-fit values were found to be $a'=9.11\pm0.28$ and $b'=14.3\pm1.0$. The dashed lines in Fig. 7 represent the results of linear regressions applied to the sets of data points with the given i or Z_2, while the solid lines represent the predictions of Eq. (6).

Satellite peak shifts relative to their corresponding diagram lines can be obtained by adding the calculated satellite shifts for zero outer-shell vacancies to the shifts due to outer-shell vacancies, ΔE^i (Z_2), given by Eq. (6). Based on the results of the MCDF calculations performed for a representative set of target atoms ($Z_2=17,19,22,23,27,28,29$), it was found that the satellite shifts for zero outer-shell vacancies can be represented by the following semiempirical formula:

$$\Delta E_0^i(Z_2) = i(a_1 + a_2 Z_2 + a_3 i + a_4 i Z_2), \tag{7}$$

in which $a_1=-11.64\pm0.41$, $a_2=1.493\pm0.017$, $a_3=0.755\pm0.071$, and $a_4=-0.0112\pm0.0030$. The rms deviation of the values obtained using the atomic structure calculations from those obtained with Eq. (7) was found to be 0.55 eV.

Systematic trends of x-ray satellite energy shifts have been studied previously by Török, Papp, and Raman [19]. However, in that study, the dependence on p_L^x was neglected. By comparing their recommended satellite shifts with the predictions obtained from Eq. (6), one can infer, for each i, the average value of p_L^x that characterized the x-ray spectra on which their compilation was based. Generally, that average value of p_L^x increases with i. This is not unexpected, since satellite energy shifts corresponding to high values of i and small p_L^x, as well as those corresponding to small values of i and large p_L^x, are difficult to measure accurately because of their relatively small peak intensities. The recommended satellite energy shifts from Ref. [19] and the corresponding average values of p_L^x are indicated in Fig. 6 by crosses (X).

C. Gaussian component widths of the $K\alpha$ x-ray satellite peaks

In the analysis of each measured x-ray spectrum, Gaussian component widths of the Voigt peaks representing $K\alpha_1 L^i$ or $K\alpha_2 L^i$ satellite transitions were assumed to be the same

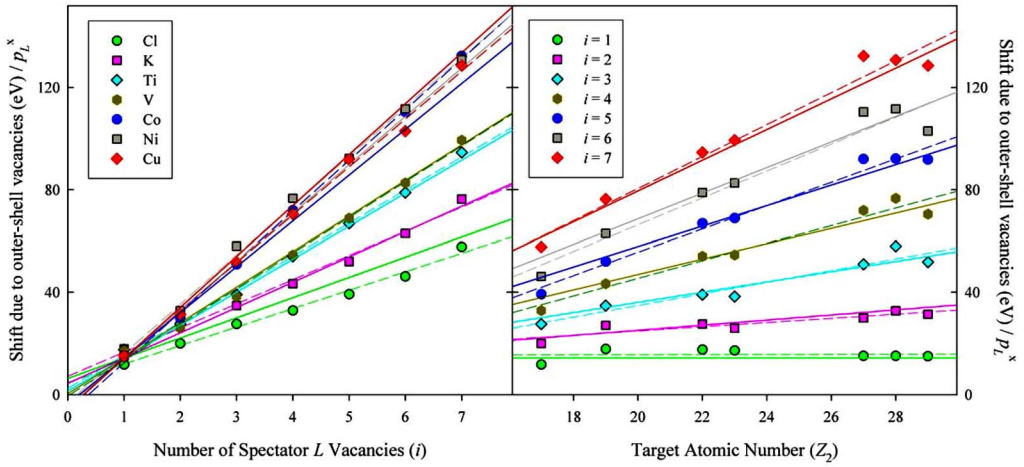

FIG. 7. (Color online) Energy shift of $K\alpha$ satellite peaks due to outer-shell vacancies divided by the apparent average L-vacancy fraction at the time of $K\alpha$ x-ray emission (p_L^x) as a function of the associated number of spectator L vacancies (i) and the target atomic number (Z_2). (See text for details.)

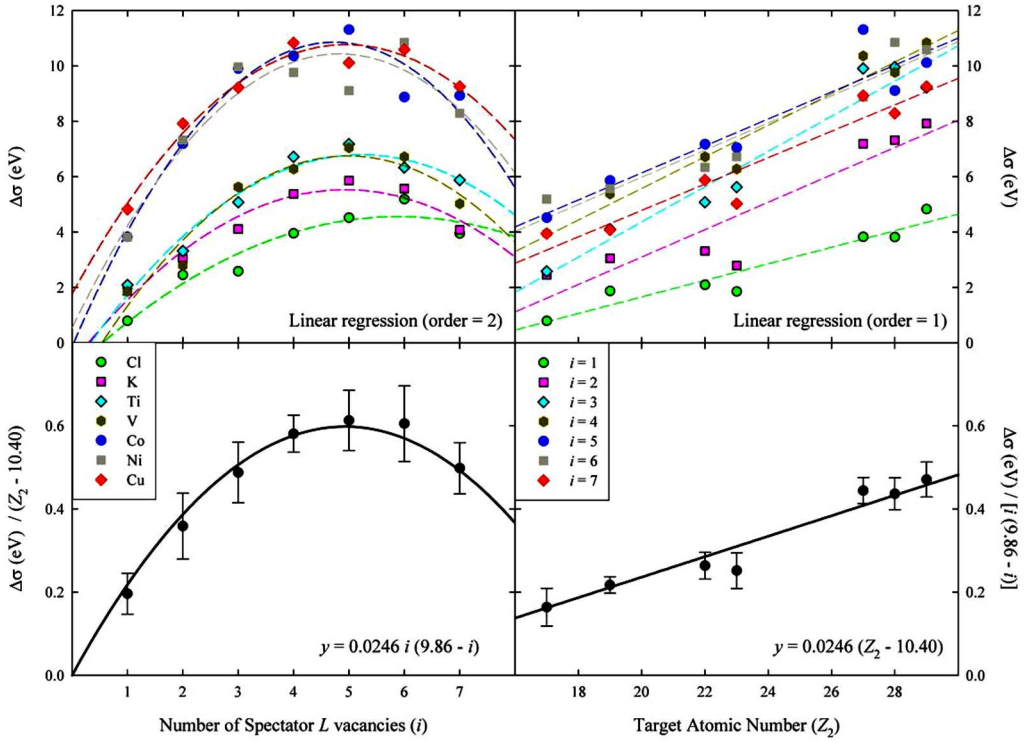

FIG. 8. (Color online) Dependence of the satellite peak widths in excess of the instrumental resolution ($\Delta\sigma$) on the associated number of spectator L vacancies (i) and the target atomic number (Z_2). The error bars represent sample standard deviations. (See text for details.)

for a given i. For different values of i, whenever possible, these widths were determined as independent parameters of the fit, without additional constraints. This procedure was justified by the fact that each satellite peak width is determined primarily by the distribution of a large number of unresolved transitions having a range of transition energies. The spread of transition energies is due to the coupling of electronic angular momenta in the initial and final states, as well as the probability distribution of outer-shell vacancy configurations. The Gaussian component widths of satellite peaks that were not resolved from other peaks and represented a relatively small fraction of the satellite peak distribution could not be determined as independent parameters of the fit. Instead, their values were estimated and held constant. However, they were *not* included in the analysis described below.

Independently determined Gaussian component widths of the satellite peaks were grouped according to their associated numbers of spectator L vacancies (i) and the target atomic number (Z_2), regardless of the projectile atomic number and projectile energy. The data in each group were then replaced by their average value $\sigma_s(i,Z_2)$. A similar procedure was applied to the Gaussian component widths of the diagram peaks by sorting them in groups based on Z_2 and then replacing the widths in each group by their average value $\sigma_d(Z_2)$. The differences $\Delta\sigma(i,Z_2)=\sigma_s(i,Z_2)-\sigma_d(Z_2)$ are shown in Fig. 8 on the top left and top right, as a function of i and Z_2, respectively. The curves in the graphs represent the results of unconstrained linear regressions applied to each individual set of data with the given i or Z_2. Based on the trends observed in the two graphs, it was found that $\Delta\sigma(i,Z_2)$ can be approximated by

$$\Delta\sigma(i,Z_2) = a''i(b''-i)(Z_2-c''), \tag{8}$$

where a'', b'', and c'', are constants. Their best-fit values were found to be $a''=0.0246\pm0.0018$, $b''=9.86\pm0.23$, and $c''=10.40\pm0.74$. The graphs on the bottom left and bottom right of Fig. 8 illustrate how well the data points are represented by Eq. (8). On the bottom left, $\Delta\sigma(i,Z_2)/(Z_2-c'')$ is plotted as a function of i, while on the bottom right, $\Delta\sigma(i,Z_2)/[i(b''-i)]$ is plotted as a function of Z_2. The data points in these graphs represent the average values of all the derived data points at the given value of the abscissa, while the error bars represent sample standard deviations.

Widths of the Gaussian peaks representing $K\alpha$ x-ray satellites have been studied previously by Banaś *et al.* [20]. However, in that study, the measurements were performed using a semiconductor x-ray detector. Consequently, the satellite peaks corresponding to different values of i were not resolved and the effort was focused on parametrizing the width of the entire satellite peak distribution (i.e., the combined contribution from satellite peaks corresponding to all values of i, convolved with a substantial instrumental width).

VI. CONCLUSION

Spectra $K\alpha$ x-rays excited in collisions spanning a wide range of heavy-ion projectiles, collision energies, and targets have been measured using a curved crystal spectrometer. Comprehensive analyzes of these spectra have revealed systematic dependencies on the collision parameters of important spectral features associated with multiple vacancy production. Specifically, the following observations have

evolved from this work: (a) The apparent average L-shell spectator vacancy fraction at the time of $K\alpha$ x-ray emission, p_L^x, was found to be a universal function of the Geometrical Model's parameter X_n. This experimentally determined function [Eq. (5)], however, deviates substantially from the theoretical predictions. (b) For a given target, the centroid of each $K\alpha$ satellite peak was found to vary linearly with p_L^x, regardless of the projectile atomic number (Z_1) and energy. This behavior indicates that the degree of outer-shell ionization in K-shell ionizing collisions is directly correlated with the degree of simultaneous L-shell ionization. (c) The Gaussian component widths of the $K\alpha$ satellite peaks were found to vary systematically with the target atomic number (Z_2) and the number of spectator L vacancies.

One practical outcome of the present work is that it provides a means of estimating the various spectral parameters for collisions of projectiles having $Z_1=6$ to 83 with solid targets of elements with $Z_2=17$ to 32 at energies in the range of 2.5 to 25 MeV/amu. Using the empirical formulas presented herein together with the diagram line natural widths [11] and the instrumental resolution, a complete representation of the $K\alpha$ x-ray satellites may be obtained. Finally, the relative intensities of the diagram lines may be estimated by employing the methods discussed in Refs. [9,10] to account for contributions from secondary ionization processes.

ACKNOWLEDGMENT

This work was supported by the Robert A. Welch Foundation.

[1] B. Perny, J.-Cl. Dousse, M. Gasser, J. Kern, Ch. Rheme, P. Rymuza, and Z. Sujkowski, Phys. Rev. A **36**, 2120 (1987).
[2] D. F. Anagnostopoulos, G. Borchert, D. Gotta, K. Rashid, D. H. Jakubassa-Amundsen, and P. A. Amundsen, Phys. Rev. A **58**, 2797 (1998).
[3] C. Schmiedekamp, B. L. Doyle, T. J. Gray, R. K. Gardner, K. A. Jamison, and P. Richard, Phys. Rev. A **18**, 1892 (1978).
[4] R. L. Watson, B. I. Sonobe, J. A. Demarest, and A. Langenberg, Phys. Rev. A **19**, 1529 (1979).
[5] H. F. Beyer, R. Mann, and F. Folkmann, Nucl. Instrum. Methods Phys. Res. **202**, 177 (1982).
[6] B. Sulik, I. Kadar, S. Ricz, D. Varga, J. Vegh, G. Hock, and D. Berenyi, Nucl. Instrum. Methods Phys. Res. B **28**, 509 (1987).
[7] J. H. McGuire and P. Richard, Phys. Rev. A **8**, 1374 (1973).
[8] R. D. Deslattes, E. G. Kessler, P. Indelicato, L. de Billy, E. Lindroth, and J. Anton, Rev. Mod. Phys. **75**, 35 (2003).
[9] R. L. Watson, J. M. Blackadar, and V. Horvat, Phys. Rev. A **60**, 2959 (1999).
[10] V. Horvat and R. L. Watson, J. Phys. B **34**, 777 (2001).
[11] J. L. Campbell and T. Papp, At. Data Nucl. Data Tables **77**, 1 (2001).
[12] S. I. Salem, S. L. Panossian, and R. A. Krause, At. Data Nucl. Data Tables **14**, 91 (1974).
[13] J. P. Desclaux, Comput. Phys. Commun. **9**, 31 (1975).
[14] J. H. McGuire and P. Richard, Phys. Rev. A **8**, 1374 (1973).
[15] V. Horvat, R. L. Watson, J. M. Blackadar, A. N. Perumal, and Yong Peng, Phys. Rev. A **71**, 062709 (2005).
[16] F. Ziegler (1996), *program SRIM* (http://www.srim.org/).
[17] W. Brandt and G. Lapicki, Phys. Rev. A **23**, 1717 (1981); G. Lapicki and F. D. McDaniel, *ibid.* **22**, 1896 (1980).
[18] M. J. Berger, J. H. Hubbell, S. M. Seltzer, J. Chang, J. S. Coursey, R. Sukumar, and D. S. Zucker, *program XCOM* (http://physics.nist.gov/PhysRefData/Xcom/Text/XCOM.html).
[19] I. Torok, T. Papp, and S. Raman, Nucl. Instrum. Methods Phys. Res. B **150**, 8 (1999).
[20] D. Banas, J. Braziewicz, U. Majewska, M. Pajek, J. Semaniak, T. Czyzewski, M. Jaskola, W. Kretschmer, and T. Mukoyama, Nucl. Instrum. Methods Phys. Res. B **154**, 247 (1999).